JOURNAL OF
THE ENGINEERING
MECHANICS DIVISION

# BLUNT CRACK BAND PROPAGATION IN FINITE ELEMENT ANALYSIS

By Zdeněk P. Bažant[1] and Luigi Cedolin,[2] Members, ASCE

## NATURE OF PROBLEM

In the current practice of finite element analysis of concrete structures, as well as rocks, cracks are considered to be densely distributed (smeared) throughout the finite area of the element (4,17,22,24). The assumption of continuous crack distribution seems reasonable in view of material inhomogeneity and the stabilizing effect of reinforcement, although at the final stage of failure the cracks certainly tend to localize into isolated sharp cracks (1).

The smeared crack concept has significant practical advantages, too. Its programming requires merely an adjustment of element stiffness. This is far simpler than programming for the alternative approach of isolated sharp interelement cracks, in which one must cope with topological changes in element connectivity, a complication that is likely to lead to inefficient codes.

Perhaps the most compelling reason for using a smeared crack band of a blunt front is that one can easily consider cracks of *any* direction and one pays no penalty when the crack direction is unknown. On the other hand, a directional change of a sharp interelement crack requires changing the coordinates of nodes, which is particularly cumbersome if the crack direction is unknown. Smeared cracks can also exhibit without any difficulties crack branching that is unknown in advance. Indeed, the practical advantages of the smeared crack concept are often so overwhelming that its use may be effective even for treating cracks that are actually sharp and isolated, as in homogeneous materials.

As presently used, however, the smeared crack concept suffers from one fundamental drawback. The crack band is normally assumed to propagate into

Note.—Discussion open until September 1, 1979. To extend the closing date one month, a written request must be filed with the Editor of Technical Publications, ASCE. This paper is part of the copyrighted Journal of the Engineering Mechanics Division, Proceedings of the American Society of Civil Engineers, Vol. 105, No. EM2, April, 1979. Manuscript was submitted for review for possible publication on April 25, 1978.

[1]Prof. of Civ. Engrg., Northwestern Univ., Evanston, Ill.

[2]Visiting Scholar, Northwestern Univ., Evanston, Ill.; on leave as Assoc. Prof., Politecnico di Milano, Milano, Italy.





the next finite element when the stress in this element reaches a specified strength. The magnitude of this stress depends on the sharpness of the front of the crack band and, in particular, the width of the front element of the blunt crack band. The smaller this width is chosen, the larger is the stress in the element just ahead of the front, and the smaller is the applied load that causes propagation. In the limit, if the element width shrinks to zero, the stress in the element just ahead of the crack front becomes infinite for any finite load value, which indicates that the crack would propagate at nearly zero load (1). This is obviously incorrect.

The simplest way to eliminate the spurious dependence of propagation on the chosen finite element width is to use fracture mechanics criteria of crack

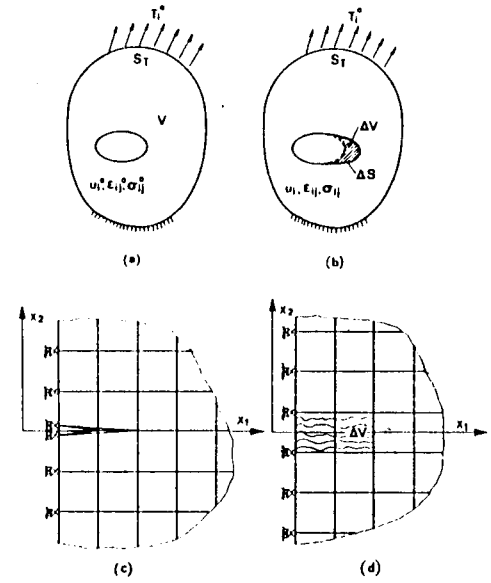


**FIG. 1.—(*a*) Notch in Elastic Continuum; (*b*) Advance; (*c*) Sharp Interelement Crack in Finite Element Mesh; (*d*) Blunt Crack Band in Finite Element Mesh**

propagation in concrete (8,11,23,26). These are expressed in terms of the energy needed for crack extension, a quantity that is independent of the size of the front element, provided the element is small enough. Thus, even though the applicability of fracture mechanics criteria to cracking of concrete bodies of small size is debatable (26), their use is preferable for reasons of the principle of objectivity in mechanics of materials (as long as more sophisticated models to treat crack localization are unavailable). The existing finite element codes based on fracture mechanics use, however, isolated sharp cracks located at element interfaces, which is not only unrealistic for concrete, but also less simple to use and less efficient from the programming viewpoint, especially when the crack direction is unknown.

The aim of this paper is to show a possibility of using the fracture mechanics

propagation criteria in conjunction with the highly efficient smeared crack concept. The use of singularity elements will be avoided and three methods of different merits will be proposed and explored. In one method, the energy flow into the crack front during the advance of the blunt smeared crack band into the next element will be calculated in terms of quantities referring to the cracked zone itself, and the critical value of the applied load will be determined from these quantities. In the second method, a propagation criterion equivalent to fracture mechanics but expressed in terms of the stress in the element ahead of the crack front will be investigated. Finally, in the third method, the stress intensity factor of an equivalent sharp crack will be calculated by fitting the asymptotic series expansion of the sharp crack displacement field to the nodal displacements near the crack front.

## Method A—Energy Variation Due to Crack Advance

**Crack Advance in Elastic Continuum.**—Before turning attention to finite elements, we must first calculate the change of energy due to crack advance in a continuum. This has been done by Rice (21), and we will first briefly review it to set the stage. For the sake of brevity, we will restrict attention to elastic solids, even though this is not inevitable.

Consider a body that contains a notch [Fig. 1(*a*)] and is loaded by surface tractions $T_i^o$ on its boundary $S_T$. Let $u_i^o$, $\epsilon_{ij}^o$, and $\sigma_{ij}^o$ denote the displacements, strains, and stresses in this initial state. Consider now a static notch extension in which, while the loading remains constant, the notch increases by $\Delta V$ in volume [Fig. 1(*b*)], creating a new traction-free surface $\Delta S$. Let $u_i$, $\epsilon_{ij}$, and $\sigma_{ij}$ denote the new values of displacements, strains, and stresses. The potential energy of tractions $T_i^o$ that initially exists at surface $S_T$ is $-\int_{S_T} T_i^o u_i^o\, dS$, and so the total potential energy is

$$U^o = \frac{1}{2}\int_V \sigma_{ij}^o \epsilon_{ij}^o\, dV - \int_{S_T} T_i^o u_i^o\, dS \quad \ldots\ldots\ldots\ldots\ldots\ldots\ldots\ldots (1)$$

in the initial state, while

$$U = U^o + \Delta U = \frac{1}{2}\int_{V-\Delta V} \sigma_{ij}\epsilon_{ij}\, dV - \int_{S_T} T_i^o u_i\, dS \quad \ldots\ldots\ldots\ldots\ldots (2)$$

in the final state. (Repeated indices imply summation over $i, j = 1, 2, 3$.) Thus, the potential energy increment is

$$\Delta U = -\frac{1}{2}\int_{\Delta V} \sigma_{ij}^o \epsilon_{ij}^o\, dV + \frac{1}{2}\int_{V-\Delta V} (\sigma_{ij}\epsilon_{ij} - \sigma_{ij}^o\epsilon_{ij}^o)\, dV$$

$$- \int_{S_T} T_i^o (u_i - u_i^o)\, dS \quad \ldots\ldots\ldots\ldots\ldots\ldots\ldots\ldots\ldots (3)$$

Since the body is elastic, $\Delta U$ is the same for any path of transition between the two states. In this light, consider that the body first passes to an intermediate state in which the volume $\Delta V$ of material is removed from the body, but surface tractions $T_i^o = \sigma_{ij}^o n_j$ are applied to the newly formed surface $\Delta S$ in order to



preserve the initial state of deformation within the remaining part of the body. Then the change of the total potential energy is equal to the elastic energy initially contained within $\Delta V$

$$\Delta W_{(\Delta V)} = -\frac{1}{2}\int_{\Delta V} \sigma_{ij}^o \epsilon_{ij}^o\, dV \quad \ldots\ldots\ldots\ldots\ldots\ldots\ldots\ldots\ldots (4)$$

which coincides with the first term of Eq. 3. Subsequently, the tractions $T_i^o$ applied on $\Delta S$ are released. This second part of the transition, which leads to the final state, produces an increase of the elastic energy within the volume $V - \Delta V$ and a decrease of the potential energy of the surface tractions on $S_T$ expressed, respectively, by the second and third term of Eq. 3. Applying the theorem of virtual displacements to this second part of the transition, we find that the strain-energy change within $V - \Delta V$ equals the work of $T_i^o$ on $S_T$ and on $\Delta S$, i.e.,

$$\frac{1}{2}\int_{V-\Delta V} (\sigma_{ij}\epsilon_{ij} - \sigma_{ij}^o\epsilon_{ij}^o)\, dV = \int_{S_T} T_i^o (u_i - u_i^o)\, dS$$

$$+ \frac{1}{2}\int_{\Delta S} T_i^o (u_i - u_i^o)\, dS \quad \ldots\ldots\ldots\ldots\ldots\ldots\ldots\ldots\ldots (5)$$

in which the last term has coefficient 1/2 because $T_i^o$ is reduced to 0 on $\Delta S$ while changing negligibly on $S_T$ because $u_i$ and $u_i^o$ are infinitesimal.

Substituting Eq. 5 into Eq. 3 and taking into account Eq. 4, we obtain

$$\Delta U = \Delta W_{(\Delta V)} + \frac{1}{2}\int_{\Delta S} T_i^o (u_i - u_i^o)\, dS \quad \ldots\ldots\ldots\ldots\ldots\ldots (6)$$

which allows the variation of the total potential energy to be calculated solely in terms of quantities defined in the vicinity of the notch tip.

**Crack Advance in Finite Element Mesh.**—One possible way of representing crack propagation in finite element analysis consists of disconnecting the nodes of adjacent elements, as indicated in Fig. 1(*c*). The practical alternative, which is advantageous for reasons already explained, is to smear the crack over a finite zone $\Delta V$, which may coincide with an element, as represented in Fig. 1(*d*), or with several elements. Zone $\Delta V$ is assumed to retain only the capability of transmitting the normal stress $\sigma_{11}$, parallel to the crack direction. Using the previous notation also for the finite element model, we must modify the formulation in order to take into account the fact that the volume element $\Delta V$ (the element ahead of the crack) is not removed but only changes its elastic properties.

Consider again the transition from the initial uncracked state to the final cracked state. The energy loss in element $\Delta V$ becomes

$$-\frac{1}{2}\int_{\Delta V} (\sigma_{ij}^o\epsilon_{ij}^o - \sigma_{11}\epsilon_{11})\, dV = -\frac{1}{2}\int_{\Delta V} (\sigma_{ij}^o\epsilon_{ij}^o - E'\epsilon_{11}^2)\, dV \quad \ldots\ldots\ldots (7)$$

in which $E'$ is the elastic modulus for $d\epsilon_{11}$ at $\sigma_{22} = 0$, i.e., $E' = E =$ Young's modulus, in case of plane stress. It may be imagined that the element $\Delta V$ becomes equivalent to a set of springs in direction $x_1$, parallel to the crack,

while before cracking it had the properties of a two-dimensional continuum. For the case of plane strain we have $E' = E/(1 - \nu^2)$ in which $\nu$ = Poisson ratio, in which case the transverse planes $(x_1, x_3)$ are, after cracking, in the plane stress state. Eq. 3, which expresses the variation of the total potential energy, becomes

$$\Delta U = -\frac{1}{2}\int_{\Delta V}(\sigma^o_{ij}\epsilon^o_{ij} - E'\epsilon^{o2}_{11})\,dV + \frac{1}{2}\int_{V-\Delta V}(\sigma_{ij}\epsilon_{ij} - \sigma^o_{ij}\epsilon^o_{ij})\,dV - \int_{S_T} T^o_i(u_i - u^o_i)\,dS \quad \ldots\ldots\ldots\ldots\ldots\ldots\ldots\ldots (8)$$

This expression could be used to calculate $\Delta U$ but would be inefficient. A more efficient calculation is possible, since $\Delta U$ can be expressed only in terms of the quantities defined in $\Delta V$ and $\Delta S$. It is again useful to consider an intermediate state in which the material in the remaining part, $V - \Delta V$, of the body is kept in its initial state by means of surface tractions externally applied on $\Delta S$. The energy variation during the transition from the initial state to this intermediate state no longer coincides with the total energy initially contained in $\Delta V$, but is expressed as

$$\Delta W_{(\Delta V)} = -\frac{1}{2}\int_{\Delta V}(\sigma^o_{ij}\epsilon^o_{ij} - E'\epsilon^{o2}_{11})\,dV \quad \ldots\ldots\ldots\ldots\ldots\ldots\ldots\ldots (9)$$

The strain in element $\Delta V$ in the intermediate state remains equal to the initial one while the material properties are changed. Term $E'/\epsilon^{o2}_{11}$ represents the density of the energy that remains in $\Delta V$. The surface forces $\Delta T_i$, which must be externally applied on $\Delta S$ to the remaining part, $V - \Delta V$, of the body in order to preserve the initial stress state, are those that result from the following stress decrements in $\Delta V$:

$$\Delta\sigma_{11} = \sigma^o_{11} - E'\epsilon^o_{11} = \frac{E'}{1-\nu'^2}(\epsilon^o_{11} + \nu'\epsilon^o_{22}) - E'\epsilon^o_{11}; \quad \Delta\sigma_{22} = \sigma^o_{22}; \quad \Delta\sigma_{12} = \sigma^o_{12} \quad \ldots\ldots\ldots\ldots\ldots\ldots\ldots\ldots (10)$$

in which $\nu' = \nu$ for plane stress; and $\nu' = \nu/(1 - \nu)$ for plane strain.

Now let the surface forces $\Delta T_i$ corresponding to these stresses on the surface $\Delta S$ of element $\Delta V$ be statically removed. The virtual work relation for this second part of transition is similar to Eq. 5, but it includes an additional term, the energy change within the volume $\Delta V$ due to the release of surface forces $\Delta T_i$, i.e.

$$\frac{1}{2}\int_{\Delta V}(\sigma_{11}\epsilon_{11} - E\epsilon^{o2}_{11})\,dV + \frac{1}{2}\int_{V-\Delta V}(\sigma_{ij}\epsilon_{ij} - \sigma^o_{ij}\epsilon^o_{ij})\,dV = \int_{S_T} T^o_i(u_i - u^o_i)\,dS + \frac{1}{2}\int_{\Delta S}\Delta T_i(u_i - u^o_i)\,dS \quad \ldots\ldots\ldots\ldots\ldots\ldots (11)$$

Substituting Eq. 11 into Eq. 8 and taking into account Eq. 9 and the relation $\sigma_{11} = E'\epsilon_{11}$, one obtains again Eq. 6 in which $\Delta W_{(\Delta V)}$ is the energy loss that occurs in the transition to the intermediate state, i.e.



$$\Delta U = -\frac{1}{2}\int_{\Delta V}(\sigma^o_{ij}\epsilon^o_{ij} - E'\epsilon^{o2}_{11})\,dV + \frac{1}{2}\int_{\Delta S}\Delta T_i(u_i - u^o_i)\,dS \quad \ldots\ldots\ldots\ldots\ldots\ldots\ldots\ldots (12)$$

The first term represents the energy loss in $\Delta V$ due to the change in elastic moduli matrix while the second term represents the effect of the release of $\Delta T_i$ for the *entire* body $V$. (The surface forces that exist on $\Delta S$ can be practically evaluated from the stiffness matrix of volume $\Delta V$ and its displacements.)

**Calculation of Stress Intensity Factor.**—Using Eq. 12, the potential energy-release rate at crack extension, $\mathcal{J} = \partial U/\partial a$, can be approximated as

$$\mathcal{J} = (\mathcal{J})_{a+\Delta a/2} = \frac{\Delta U}{\Delta a} \quad \ldots\ldots\ldots\ldots\ldots\ldots\ldots\ldots\ldots\ldots\ldots\ldots (13)$$

in which $\Delta a$ is the increment of crack length; and $\mathcal{J}$ refers to a unit thickness in $x_3$ direction. The approximation is second-order accurate if $\mathcal{J}$ is referred to crack length $a + \Delta a/2$ when $a$ is the crack length before extension $\Delta a$. Considering a symmetric (Mode I) crack opening, the stress intensity factor, $K_I$, may then be evaluated from the well-known relation (13)

$$K_I = \sqrt{E'\mathcal{J}} \quad \ldots\ldots\ldots\ldots\ldots\ldots\ldots\ldots\ldots\ldots\ldots\ldots (14)$$

The propagation condition reads $K_I = K_{cr}$ = given critical value of $K_I$ for the material at hand.

**Numerical Studies.**—To get a picture of the accuracy of the criticality predictions based on the blunt crack band method, various numerical examples whose solution is known have been run. These included a Mode I crack within an infinite medium subjected at infinity to uniaxial stress $\bar{\sigma}$ normal to the crack [Fig. 2(*a*)] and a Mode I crack located symmetrically within a finite strip of length $2L$ and width $b$ subjected to uniaxial stress $\bar{\sigma}$ at ends [Fig. 2(*b*)]. The computations have been carried out for $E' = 2{,}256\ \text{MN/m}^2$, $\nu' = 0.2$, $K_{cr} = 0.6937\ \text{MN/m}^{3/2}$. The value of the uniaxial stress applied at infinity has been fixed as $\bar{\sigma} = 0.981\ \text{MN/m}^2$ and the critical values of stress multiplier $\alpha$, giving stress $\alpha\bar{\sigma}$, have been evaluated from Eqs. 12–14 (and plotted in Fig. 3). As a check, $\Delta V$ was also calculated from Eq. 8, and the result was exactly the same as from Eq. 12. In each case, both the classical approach of a sharp interelement crack [Fig. 2(*c*)], and the present approach of a blunt smeared crack band [Fig. 2(*d*)] have been used. For the case of uniaxial tension at infinity, the distribution of the stresses to be applied along the boundary PQR in Fig. 2(*c*) or PQRS in Fig. 2(*d*) has been calculated using Westergaard's exact solution (see Ref. 2).

Only constant strain triangles have been used as finite elements in this work. Compared to finite elements with nonuniform strain their accuracy should not be as much inferior as it is in elastic analysis, because a significant error may be introduced, anyway, due to the fact that cracking is considered to spread all over the element even though the cracking criterion may be reached only in one point of the element.

Three different meshes have been utilized, with these element subdivisions: Mesh A—6 × 7, Mesh B—12 × 13, and Mesh C—16 × 25. Various crack lengths have been analyzed for each mesh. The meshes for the blunt cracks are drawn in Fig. 2(*e*). The symmetry lines A-A, B-B, and C-C indicate the

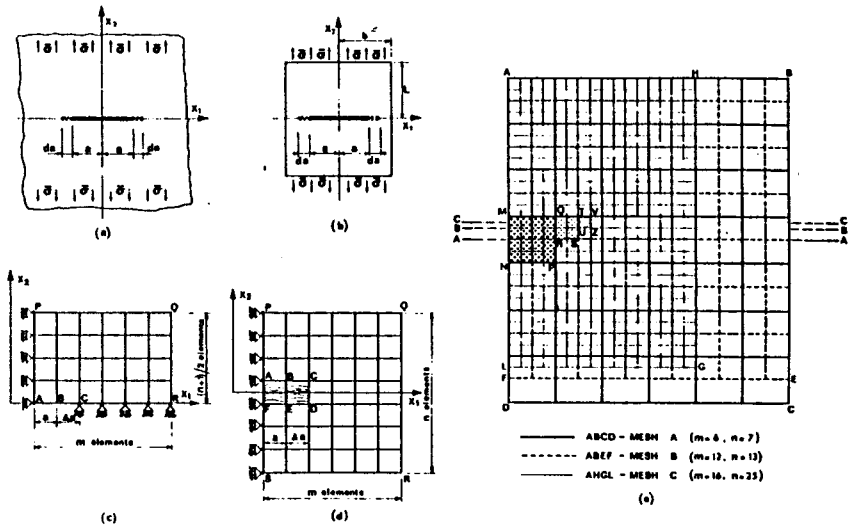


FIG. 2.—(*a*) Crack in Infinite Solid; (*b*) Crack in Finite Strip; (*c*) Finite Element Mesh Used for Sharp Interelement Crack; (*d*) Finite Element Mesh Used for Blunt-Crack Band; (*e*) Mesh Refinements Used in Examples

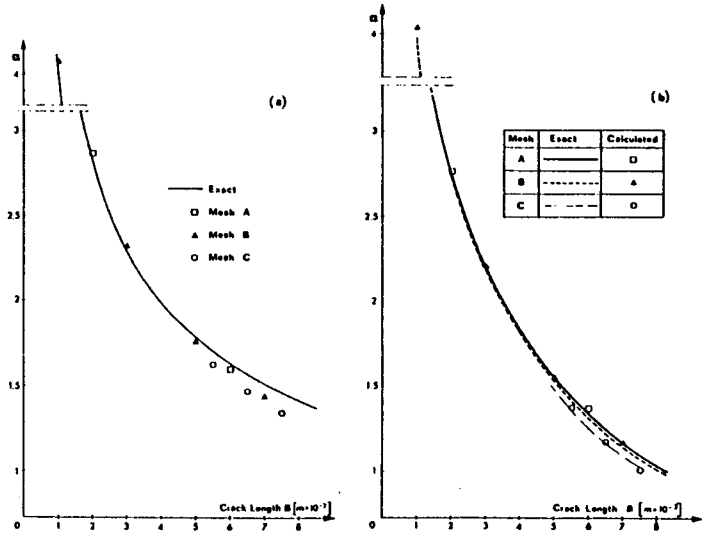


FIG. 3.—Comparison of Numerical Results from Energy Variation with Exact Solution for Blunt-Crack Band: (*a*) Infinite Solid; (*b*) Finite Strip ($\alpha$ = Load Multiplier) (1 m = 3.28 ft)



positions of the crack for each mesh, and the elements MNPQ, QRST, and TUVZ indicate the zones of the jump of the crack band during the advance

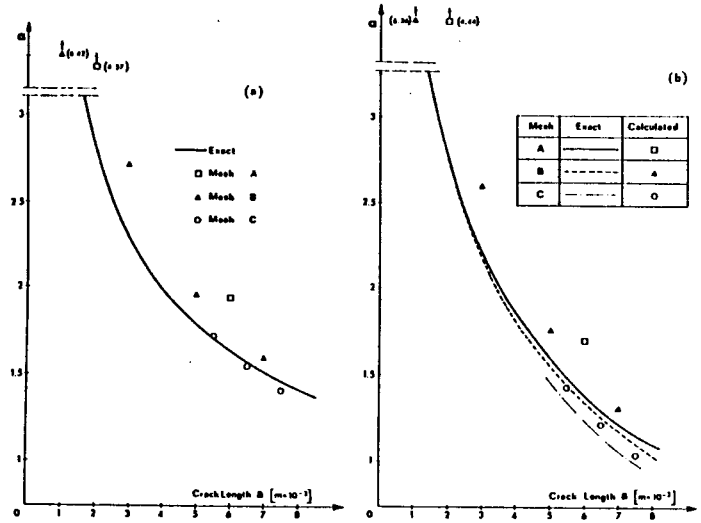


FIG. 4.—Comparison of Numerical Results from Energy Variation with Exact Solution for Sharp Interelement Crack: (*a*) Infinite Solid; (*b*) Finite Strip (1 m = 3.28 ft)

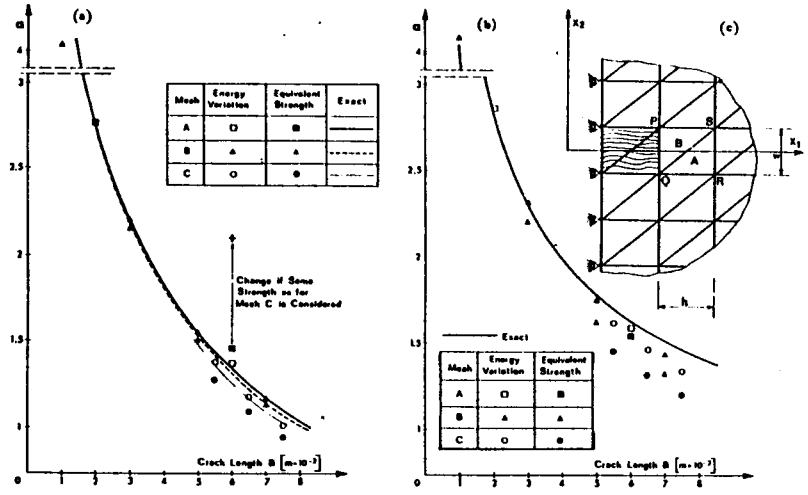


FIG. 5.—Blunt Crack Comparison between Energy Variation and Equivalent Strength Criteria: (*a*) Finite Strip; (*b*) Infinite Solid; (*c*) Mesh Detail at Front of Blunt-Crack Band (1 m = 3.28 ft)

$\Delta a$. Each square of the mesh consists of two constant-strain triangular elements. The results for the blunt smeared crack bands are exhibited in Figs. 3(*a*)

and 3(*b*). Fig. 3(*a*) is for the infinite medium, and the exact solution plotted is that of Westergaard (Refs. 27 and 13, Eq. 3.15.17). For cracks reaching only one or two elements into the coarse mesh, good accuracy, in general, cannot be expected. Curiously, the present results are good, however, even for these cases [Fig. 3(*a*)], which must be considered particular to this example. In Fig. 3(*b*), similar comparisons are made for the finite strip, for which a highly accurate solution is known (14,25). (These solutions are different for each mesh because each mesh corresponds to a slightly different length-to-width ratio of the specimen.)

Comparable results for a sharp interelement crack are given in Figs. 4(*a*) and 4(*b*). For the finest mesh, the sharp crack agrees with the exact solution better than the blunt crack band [Fig. 4(*a*)]. However, the reverse is seen to be true for the finite sheet [Fig. 4(*b*)].

The most interesting observation from Figs. 3 and 4 is that the blunt crack band gives overall about as good results as the sharp interelement crack. This might have been caused, though, by the excess stiffness of constant strain triangles. For higher-order elements, the points in Figs. 3 and 4 would undoubtedly lie somewhat lower, in which case the finite element sharp crack solution would become closer to the exact one than the blunt crack solution.

### Method B—Equivalent Strength Criterion

The preceding approach based on energy changes requires two solutions of the finite element system, each for a different length of the crack band. This represents more computational work than for the usual strength criterion that requires only one finite element solution. The use of strength criterion is, however, objectionable for reasons of spurious dependence on the chosen element size, as already mentioned. Yet, by making the strength criterion itself properly size dependent, it should be possible to offset the size dependence of the results, and this will now be attempted. This idea is partly similar to that proposed by Miyata (16).

Consider the particular mesh shown in Fig. 5(*c*), and let the advances of the crack be restricted to jumps in which both constant-strain triangles that lie ahead of the crack (*A* and *B*) are assumed to crack simultaneously. So, volume $\Delta V$ is represented by the area PQRS consisting of two elements *A* and *B*. Let us assume that the ratio of crack jump $h$ to crack band width $w$ [Fig. 5(*c*)] is fixed (e.g., $h = w$). The mean stress in crack-jump area PQRS (volume $\Delta V$) at imminent propagation may be expected to be roughly equal to the stress value calculated for the centroid of this area on the basis of the near-tip field for the critical stress intensity factor, $K_{cr}$. If $w$ is small enough, this value is proportional to $r^{-1/2}$, $r$ being the distance from the crack tip. Since $r$ is proportional to $w$, we may expect that at imminent propagation the near stress in the crack-jump region [$\Delta V$, PQRS in Fig. 5(*c*)] roughly is $\sigma_{eq} = cK_{cr}\, w^{-1/2}$, in which $c$ is some proportionality factor. We may call $\sigma_{eq}$ the equivalent stress.

However, the crack-jump region (volume $\Delta V$) would not normally be small enough, and so it is of interest to estimate $\sigma_{eq}$ with account of finite $\Delta V$. Considering the particular arrangement of elements in Fig. 5(*c*), let us neglect, for the sake of simplicity, the contributions of $\sigma^{\circ}_{11}$ and $\sigma^{\circ}_{12}$ to the strain energy



within $\Delta V$, and consider the approximation

$$\Delta W_{(\Delta V)} \approx -\frac{1}{2}\int_{\Delta V} \sigma_{22}\epsilon^{\circ}_{22}\, dV \quad \ldots\ldots\ldots\ldots\ldots\ldots\ldots\ldots\ldots\ldots \quad (15)$$

The surface fractions $\Delta T_i$ on $\Delta S$ then result from the stresses $\Delta\sigma_{11} = 0$, $\Delta\sigma_{22} = \sigma^{\circ}_{22}$, and $\Delta\sigma_{12} = 0$ in $\Delta V$. When the crack jumps into the two triangles of area $hw/2$ ahead of the crack, the energy loss according to Eq. 15 is approximately

$$\Delta W_{(\Delta V)} = -\frac{1}{2E'}\left[(\sigma^{\circ}_{22_A})^2 + (\sigma^{\circ}_{22_B})^2\right]\frac{hw}{2} \quad \ldots\ldots\ldots\ldots\ldots\ldots \quad (16)$$

in which subscripts *A* and *B* refer to elements *A* and *B*. As a further approximation, we may neglect the work of nodal forces at nodes R and S, in which case the work of nodal forces that are exerted from volume $\Delta V$ upon the rest of the body, $V - \Delta V$, is approximated as

$$\frac{1}{2}\int_{\Delta S} \Delta T_i(u_i - u^{\circ}_i)\, dS \approx -\frac{1}{4}\, h\,\sigma^{\circ}_{22_B}\left[(u_P - u^{\circ}_P) - (u_Q - u^{\circ}_Q)\right] \quad \ldots\ldots \quad (17)$$

in which $u_P$ and $u_Q$ are the displacements normal to the crack in nodes P and Q. The bracketed term represents the opening of the crack as the crack extends by one mesh step, $h$. Neglecting further $u^{\circ}_P$ and $u^{\circ}_Q$, we may approximately express $u_P - u_Q$ from the well-known near-tip displacement field of a sharp crack. Considering only the first term of the series expansion for this field (7,13,29) we have

$$u_P - u_Q \approx \frac{8}{E'}\frac{K_{cr}}{\sqrt{2\pi}}\sqrt{w} \quad \ldots\ldots\ldots\ldots\ldots\ldots\ldots\ldots\ldots\ldots \quad (18)$$

If this is substituted into Eq. 17, and if this equation is in turn substituted into Eq. 12 in which $\Delta U = h_{\mathcal{J}} = h(K_{cr})^2/E'$ (as Eqs. 13 and 14 indicate), it follows that

$$\frac{h}{E'}(K_{cr})^2 = -\frac{1}{4E'}\left[(\sigma^{\circ}_{22_A})^2 + (\sigma^{\circ}_{22_B})^2\right] hw - \sqrt{\frac{2}{\pi}}\,\frac{\sigma^{\circ}_{22_B}}{E'}\,K_{cr}\, h\sqrt{w} \quad \ldots \quad (19)$$

For a fixed arrangement of elements at the front of a blunt crack band, the ratio $\sigma^{\circ}_{22_B}/\sigma^{\circ}_{22_A}$ is roughly constant, and for the particular case in Fig. 5(*c*) one may set $\sigma^{\circ}_{22_A} \approx \sigma^{\circ}_{22_B}/2$. Substituting this into Eq. 19, we acquire a quadratic equation for $\sigma^{\circ}_{22_B}$. This equation has only one positive solution, which is of the form

$$(\sigma^{\circ}_{22_B})_{cr} = \sigma_{eq} = c\, K_{cr}\, w^{-1/2}, \quad \text{with} \quad c = 0.921 \quad \ldots\ldots\ldots\ldots\ldots \quad (20)$$

When solutions for the same fixed applied load are obtained for different crack band widths $w$, the load multiplier $\alpha$ necessary to make the crack propagate is

$$\alpha = \frac{\sigma_{eq}}{\sigma^{\circ}_{22_B}} = \frac{c}{\sigma^{\circ}_{22_B}}\, K_{cr}\, w^{-1/2} \quad \ldots\ldots\ldots\ldots\ldots\ldots\ldots\ldots\ldots\ldots \quad (21)$$

**Numerical Studies.**—Values of load multiplier $\alpha$ for blunt crack bands of various widths have been calculated from Eq. 21 as well as from the well-known accurate solutions (13,14,25,27). The results are plotted in Figs. 5(*a*) and 5(*b*) for the infinite sheet and for the finite specimen. Although numerous approximations were introduced while setting up Eq. 20, the principal trend given by Eq. 20 is seen to be correct.

By contrast, if the strength for Mesh A were considered to be the same as Mesh C, the $\alpha$ values for Mesh A [full square in Fig. 5(*a*)] would be $\sqrt{25/7}$ times larger; this is shown by point + in Fig. 5(*a*) and is seen to be in total disagreement with the correct solution.

The results in Fig. 5 confirm that finite element crack propagation solutions based on a strength criterion can indeed be made independent of the chosen element size if the strength is adjusted according to the element size. We also see that the error is large [90% in Fig. 5(*a*)] if the strength is not adjusted.

As a blunt crack band propagates through the finite element grid, the configurations and sizes of the elements ahead of the crack band tip will normally vary. If they are repetitive, however, coefficient $c$ in Eq. 20 does not have to be evaluated via Eqs. 16–19, but it can be calibrated once and for all by running one case with a known exact solution.

According to Eq. 20, $\sigma_{eq}$ varies in proportion to $w^{-1/2}$. This is, however, exact only for sufficiently small $w$. If the higher-order terms of the singular displacement field expansion were included, the dependence $\sigma_{eq} = f(w, K_{cr})$ would be more complicated.

The results in Figs. 5(*a*) and 5(*b*) also serve an instructive purpose. They demonstrate clearly that the finite element cracking analysis based on a fixed tensile strength is inherently inconsistent, for the crack band can be made at will to propagate under practically any load if a certain size of the element ahead of the crack is chosen. This fact seems to have eluded attention of many analysts who work on tensile cracking of concrete structures or rock masses.

## Method C—Fitting Asymptotic Series to Nodal Displacements

Another well-known approach that allows determining the stress-intensity factor from a single finite element solution is to fit the nodal displacements near the crack tip by an asymptotic series expansion. This has been done for sharp interelement cracks (6,10,29). When only the first square-root-singular term is included, this approach is not accurate, but better results have been obtained with a higher number of terms (12). We will now explore this approach for a blunt smeared crack band.

In the previous two methods, the actual length of crack advance and the crack direction in the continuum are no doubt poorly represented by the finite element model when the crack band jumps from element to element along a skew zig-zag path, as shown in Fig. 6(*a*). In such cases, the crack representation may be improved by picking its parameters from more remote nodes [Fig. 6(*a*), i.e., by fitting an asymptotic expansion to the nodal displacements. This makes the approach attractive for determining the crack direction. However, when the direction of crack propagation is unknown, the numerical solution becomes more difficult because the fitting ceases to be tractable by linear



regression (method of least squares). Rather, the fits must be obtained by methods of nonlinear optimization. Fortunately, very effective subroutines for such problems have recently become available in software libraries, and our idea is to take advantage of these developments.

For materials such as rock or concrete it seems that a crack can propagate only in the symmetric opening mode (Mode I), whether its path is straight or curved. We adopt the condition that the crack be of Mode I as the criterion that governs the direction of propagation for cracks of a smooth path.

Let the crack be approximately represented by the blunt crack band spreading through the mesh in Fig. 6(*a*). A typical selection of the characteristic nodes to be used for fitting the asymptotic expansion is also shown in Fig. 6(*a*). Obviously, these nodes must be neither too close nor too far from the crack front. Let $u'$, $v'$ be the displacements in coordinate system; and $x'$, $y'$ be attached to the sharp crack tip, $x'$ being the crack direction at the tip. Further, let $U$, $V$ be the displacements in the global coordinate system $X$, $Y$, and $U_T$;

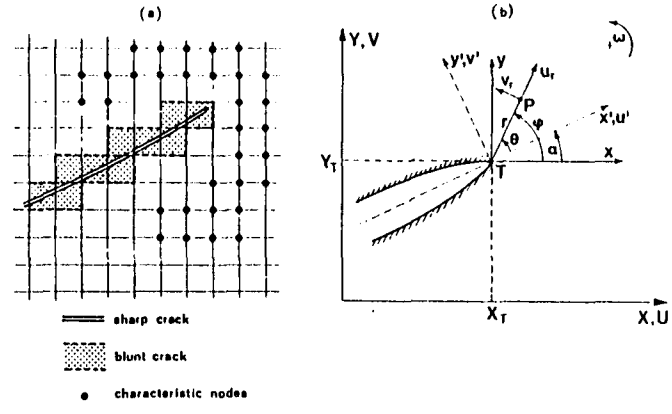


**FIG. 6.—(*a*) Blunt Crack Band of Any Direction, with Characteristic Nodes Used to Fit Asymptotic Expansion; (*b*) Coordinates for Idealized Sharp Crack Tip**

and $V_T$, $X_T$, and $Y_T$ be their values at the tip. Let us also introduce polar coordinates with regard to global axes $X$ and $Y$, i.e., $r = [(X - X_T)^2 + (Y - Y_T)^2]^{1/2}$ = the radial distance from the crack tip, and $\phi = \arctan [(Y - Y_T)/(X - X_T)]$.

Denoting the crack direction angle as $\alpha$ [Fig. 6(*b*)], we have

$$U = U_T + u' \cos\alpha - v' \sin\alpha$$

$$V = V_T + u' \sin\alpha + v' \cos\alpha \quad \ldots\ldots\ldots\ldots\ldots\ldots\ldots\ldots \quad (22)$$

It may at first appear necessary to also include in Eq. 22 the terms $-\omega_T r \sin\phi$ and $\omega_T r \cos\phi$, which are due to a small rigid body rotation, $\omega_T$, of a small neighborhood of the sharp crack tip. This would, however, be incorrect because for an idealized sharp crack whose crack surfaces are not precisely given in advance [as is the case in the mesh, Fig. 6(*a*)], it is impossible to distinguish rotation $\omega_T$ from a small change in crack direction $\alpha$. In fact, the

rigid body rotation terms were at first included in the computer program for fitting the asymptotic series to nodal displacements, but this made it impossible to achieve convergence of $\omega_T$ and $\alpha$. Note also that the same objection cannot be raised against the use of $U_T$ and $V_T$ because they represent independent nodal characteristics, separate from crack tip coordinates $X_T$ and $Y_T$, whereas in the angular sense only an angular coordinate but no particular rotation is associated with a node.

The asymptotic series expansion of stresses near a sharp crack tip has been given by Williams (28). A similar expression has been given by Gross, et al. for displacements (7), and its first four terms in terms of radial and tangential displacements $u_r$ and $v_r$ [Fig. 6(*b*)] are

$$u_r(r,\theta) = \frac{1}{2G}\sum_{n=1}^{4} [(-1)^n d_{2n-1} r^{n-(1/2)} F_1(n,\theta,\nu_o)$$

$$+ (-1)^{n+1} d_{2n} r^n F_2(n,\theta,\nu_o)];$$

$$v_r(r,\theta) = \frac{-1}{2G}\sum_{n=1}^{4} [(-1)^n d_{2n-1} r^{n-(1/2)} F_3(n,\theta,\nu_o)$$

$$+ (-1)^n d_{2n} r^n F_4(n,\theta,\nu_o)] \quad \ldots\ldots\ldots\ldots\ldots\ldots\ldots\ldots\ldots\ldots \quad (23)$$

in which $G = E'/2(1+\nu')$; $\nu_o = \nu'/(1+\nu')$; $\theta = \phi - \alpha$ = angular polar coordinate with regard to crack direction; and

$$F_1(\theta,n,\nu_o) = \left(\frac{7}{2} - n - 4\nu_o\right)\cos\left(n-\frac{3}{2}\right)\theta + \left(n-\frac{3}{2}\right)\cos\left(n+\frac{1}{2}\right)\theta;$$

$$F_2(\theta,n,\nu_o) = (3 - n - 4\nu_o)\cos(n-1)\theta + (n+1)\cos(n+1)\theta;$$

$$F_3(\theta,n,\nu_o) = \left(\frac{5}{2} + n - 4\nu_o\right)\sin\left(n-\frac{3}{2}\right)\theta - \left(n-\frac{3}{2}\right)\sin\left(n+\frac{1}{2}\right)\theta;$$

$$F_4(\theta,n,\nu_o) = -(3 + n - 4\nu_o)\sin(n-1)\theta + (n+1)\sin(n+1)\theta \quad \ldots\ldots \quad (24)$$

are the displacement eigenstates. The first two coefficients may be represented as

$$d_1 = -\frac{K_I}{\sqrt{2\pi}}; \quad d_2 = \frac{\sigma'_x}{4} \quad \ldots\ldots\ldots\ldots\ldots\ldots\ldots\ldots\ldots\ldots \quad (25)$$

in which $K_I$ = stress intensity factor; and $\sigma'_x$ = uniform uniaxial stress parallel to the crack. Furthermore

$$u' = u_r\cos\theta - v_r\sin\theta; \quad v' = u_r\sin\theta + v_r\cos\theta \quad \ldots\ldots\ldots\ldots \quad (26)$$

Eqs. 23 and 22 show that

$$U_i = U_i(U_T, V_T, X_T, Y_T, \alpha, d_1, d_2, d_3, d_4);$$

$$V_i = V_i(U_T, V_T, X_T, Y_T, \alpha, d_1, d_2, d_3, d_4) \quad \ldots\ldots\ldots\ldots\ldots\ldots \quad (27)$$

i.e., the theoretical displacements at characteristic nodes $i = 1, 2, \ldots, N$ depend on nine unknown parameters. The objective of optimum fit of the actual nodal displacements by Eqs. 22 and 23 may then be expressed by the least-square



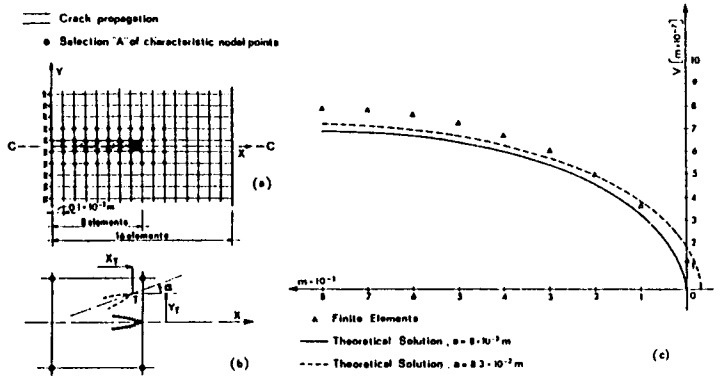


**FIG. 7.—(*a*) Example Studied by Asymptotic Expansion Fitting; (*b*) Change in Direction of Propagation; (*c*) Crack Opening Profile Obtained (1 m = 3.28 ft)**

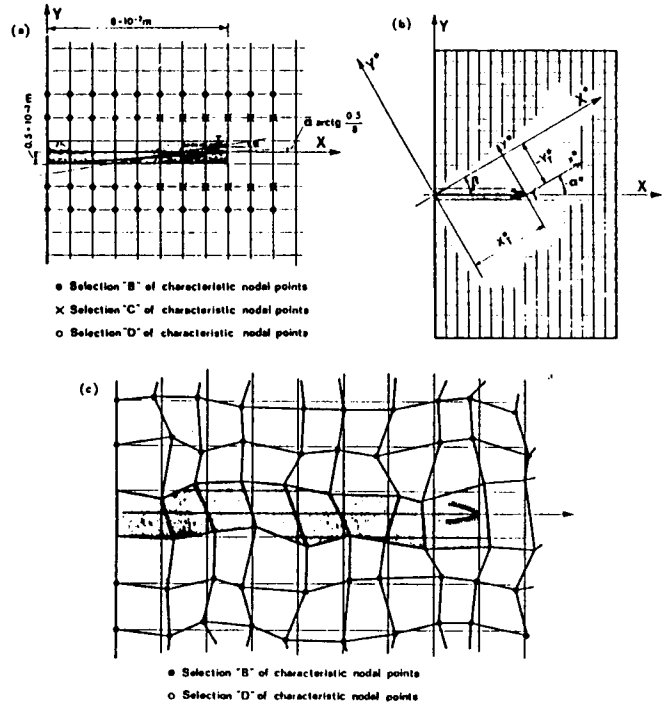


**FIG. 8.—(*a*) Various Selections of Characteristic Points; (*b*) Choice of Different Global Coordinates System; (*c*) Crack Band in Irregular Grid (1 m = 3.28 ft)**

criterion:

$$\Phi = \sum_{i=1}^{N} [w_i(U_i - \bar{U}_i)^2 + w_i(V_i - \bar{V}_i)^2] = \min \quad \ldots\ldots\ldots\ldots\ldots (28)$$

in which $\bar{U}_i$, $\bar{V}_i$ are the displacements at characteristic nodes $i = 1, 2, \ldots, N$ obtained by finite element analysis; and $w_i$ are suitably chosen weights ($w_i = 1$ has been used in all numerical runs).

The optimization problem in Eq. 28 is nonlinear because $U_i$ and $V_i$ depend nonlinearly upon crack direction $\alpha$, causing $\Phi$ to be not in a quadratic form. The nonlinear sum-of-squares problem may be solved efficiently through the use of Levenberg-Marquardt algorithm (3,15), available in most software libraries.

**Numerical Studies.**—The proposed method has been tested for the case of a blunt crack band spreading along a row of finite elements. Mesh C of Fig. 2(*e*) has been used and the case in Fig. 7(*a*) has been analyzed as an example. An idea as to how accurately the sharp crack can be represented by the blunt crack band may be obtained from Fig. 7(*c*) where the crack opening profile of the finite element mesh is compared with Westergaard's exact solution for a crack of the same length (solid line). (A somewhat better agreement is obtained when the idealized sharp crack is considered to be 0.3 element length longer than the blunt crack band; see the dashed line.)

The selection of the characteristic nodes is an important aspect of the method. One point to watch is whether during the iterations of the optimization algorithm the current $\alpha$-axis (the tangent of the crack) always remains between the nodes that are supposed to be at the opposite sides of the crack. If the characteristic points are always assigned to one or the other side of the imagined sharp crack depending on their position with regard to the $\alpha$-axis and if the $\alpha$-axis happens to move at some iteration over a nodal point, then the optimization process would fail because the point would be counted to the wrong side of the crack. To prevent this from happening, it is better not to include any nodal points that are too close to the crack band. Thus, selection A of characteristic points shown in Fig. 7(*a*) appeared to be too close and did cause the trouble just described. Selections B and C in Fig. 8(*a*) proved to be completely satisfactory from this viewpoint.

Some typical numerical results are summarized in Table 1, in which $c_i = d_i/2G$. Unless otherwise noted, the starting values for optimization were $X_T = 0.07$ m, $Y_T = 0$, $c_1 = -10^{-6}\sqrt{\text{m}}$, $c_2 = c_3 = c_4 = 0$, $U_T = -2 \times 10^{-7}$ m, $V_T = -7 \times 10^{-7}$ m, $\alpha_T = 0$, and node selection B [Fig. 8(*a*)] was used. Runs 1 and 2 merely serve to check the optimization procedure and the effect of truncating the asymptotic series. The exact displacements corresponding to biaxial tension (run 1) and uniaxial tension (run 2) at infinity are imposed at the characteristic nodes, and the results for the crack tip location $X_T$ and the stress-intensity factor (proportional to $c_1$) are satisfactory. The remaining runs in Table 1 are based on finite element results. Run 3 uses as starting values for optimization the ones previously indicated. Run 4 uses a deliberately poor initial guess, and the results are essentially the same.

Runs 5–9 are for the same crack referred to a rotated global coordinate system $X^*$ and $Y^*$ [Fig. 8(*b*)]; the results are found to be essentially unaffected by the inclination of $X^*$- and $Y^*$-axes, although the number of iterations for



optimization is higher. Runs 6–8 use the node selection C [Fig. 8(*a*)]. Run 7 starts with a much poorer initial guess ($Y_T = 0.01$ m, $\alpha = -22.9°$), but no effect on convergence is found. Run 8 uses a still poorer initial guess ($\alpha = -17.2°$). Finally, run 9, using node selection D, is based on an irregularly distorted mesh [Fig. 8(*c*)], which is found to have no significant effect on the convergence as well as the numerical results.

From Table 1 it may be noted that the obtained $K_I$ values are too high, by about 10%. The error appears to be consistent in all cases. The sign and magnitude of the error also agrees with the error in the crack opening profile [Fig. 7(*c*)] where finite elements give a greater opening than the exact solution, by about 10%. Thus, it seems that a further improvement may be possible by introducing a calibration factor to be determined by one trial run for a case of known solution.

**TABLE 1.—Typical Numerical Results for Method C**

| Run (1) | $N_r$ (2) | $X_T$, in centimeters (3) | $Y_T$, in centimeters (4) | $U_T \times 10^5$, in centimeters (5) | $V_T \times 10^5$, in centimeters (6) | $\alpha$, in degrees (7) | $c_1 \times 10^5$, in centimeters$^{1/2}$ (8) | $c_2 \times 10^5$ (9) | $c_3 \times 10^5$, in centimeters$^{1/2}$ (10) | $c_4 \times 10^5$, in centimeters$^{-1}$ (11) |
|---|---|---|---|---|---|---|---|---|---|---|
| *E* | — | 8.0 | 0.0 | −2.5 | −9.0 | 0.0 | −1.0434 | — | — | — |
| 1 | 36 | 7.8642 | — | — | — | — | −1.0752 | 0.0516 | 0.0433 | −0.0015 |
| 2 | 36 | 7.8642 | — | — | — | — | −1.0752 | −0.0788 | 0.0433 | −0.0015 |
| 3 | 55 | 7.8858 | −0.0567 | −3.8186 | −9.3917 | −0.07 | −1.1906 | −0.1474 | 0.0439 | 0.0006 |
| 4 | 55 | 7.8863 | −0.0567 | −3.8183 | −9.3917 | −0.07 | −1.1904 | −0.1473 | 0.0439 | 0.0006 |
| *E** | — | 7.0200 | −3.835 | −6.508 | −6.69 | −28.64 | −1.0434 | — | — | — |
| 5 | 101 | 6.8933 | −3.8304 | −7.8537 | −6.4113 | −28.72 | −1.1906 | −0.1473 | 0.0439 | 0.0007 |
| 6 | 55 | 6.8364 | −3.8035 | −7.8515 | −6.4134 | −28.70 | −1.2030 | −0.1489 | 0.0454 | 0.0008 |
| 7 | 52 | 6.9264 | −3.8234 | −7.8204 | −6.409 | −29.02 | −1.1564 | −0.1329 | 0.0326 | −0.0017 |
| 8 | 54 | 6.9271 | −3.8253 | −7.8205 | −6.409 | −29.00 | −1.1556 | −0.1327 | 0.0325 | −0.0017 |
| 9 | 76 | 6.8530 | −3.9707 | −8.293 | −6.739 | −28.59 | −1.2852 | −0.1587 | 0.0494 | 0.0013 |

Note: $N_r$ = number of evaluations of Eq. 28; *E* = exact values for runs 1–4; *E** = exact values for runs 5–9.

## Comparison and Analysis of Methods

Method B is the simplest one and is closest to the present practice. Method A is clearly more accurate than method B but it is also more costly and requires more involved programming. Method C is still more complicated for programming, has higher computation costs than the other two methods, and is less accurate than method A, but it seems to be most effective for accurately representing the direction of crack propagation in the continuum when this direction is oblique with regard to the mesh. For methods B and C, the theoretical crack direction in the continuum is not represented accurately if the crack jumps from element to element in a zig-zag path [Fig. 7(*a*)].

The overall accuracy of the results must be judged keeping in mind that only rather crude meshes have been employed and only the simplest finite elements, the constant-strain triangles, have been used. The use of higher-order finite elements outside the crack band would undoubtedly improve the accuracy.

Extensions to nonlinear material behavior will become important in future work. Methods B and C are inapplicable for this purpose while method A could

possibly be extended, although not in the Griffith sense based on energy flux into an idealized sharp crack tip (20). Rather, the energy dissipation at the front of the advancing blunt crack band must be considered to represent the actual fracture process; this may be accomplished if the width of the crack band and the length of the crack advance needed to reduce the stresses to zero are considered as material properties to be derived from experiments.

The need in Method A for two solutions could be eliminated by directly calculating the derivative of the stiffness matrix with respect to the crack length, as in Refs. 9 and 19. However, such calculation would not provide the stress and displacement fields.

Finally, we must realize that, due to crack surface roughness, a crack in concrete or rock can transmit compressive and shear stress if there is a small tangential movement. This is a consequence of crack dilatancy due to aggregate interlock at shear loading. For general fracture problems, these phenomena would have to be included.

## Summary and Conclusions

Modeling crack propagation by means of cracks that are distributed (smeared) within the finite elements is simpler than by means of sharp interelement cracks and is particularly attractive when the direction of the crack is unknown or crack branching occurs. For concrete and rock, a smeared crack band of a blunt front is also physically more realistic than a sharp crack.

The widely used strength criterion is not objective because the crack band can be made to propagate under any load if the size of the elements at the front of the blunt crack band is made small enough.

Three objective methods, which avoid the use of singularity elements, are proposed. In method A, the energy-release rate for the extension of the blunt crack band is calculated from the strain energy change within the element into which the crack band spreads and the work of nodal forces that are released at the nodes of this element. In method B, the stress-intensity factor is determined from the stress in the element just ahead of the crack band front, and a method of determining an equivalent strength from the element size and the given stress-intensity factor is developed. In method C, it is assumed that the crack propagation direction is such that the crack be of pure Mode I; nodal displacements near the front of the crack band are fitted by the asymptotic series expansion for the crack tip, using a nonlinear optimization subroutine. The last method is most accurate for determining the crack direction, but it is also most complicated. Method B is most effective numerically. Method A is more accurate than methods B and C. Comparisons with exact solutions of example problems are satisfactory. Method A seems to be the most suited to extension to nonlinear material behavior, while methods B and C are inapplicable. If a fixed strength value is used, a large error (e.g., 90%) can be committed.

## Acknowledgment

Support of the National Science Foundation under grants ENG 75-14848 and ENG 75-14848 A01 to Northwestern University and of the Consiglio Nazionale delle Ricerche of Italy is gratefully acknowledged. Thanks are also due to John Simon Guggenheim Foundation for supporting part of the work by awarding Guggenheim Fellowship to the first writer.



## Appendix.—References

1. Bažant, Z. P., "Instability, Ductility, and Size Effect in Strain-Softening Concrete," *Journal of the Engineering Mechanics Division*, ASCE, Vol. 102, No. EM2, Proc. Paper 12042, Apr., 1976, pp. 331–344.
2. Bažant, Z. P., Glazik, J. L., and Achenbach, J. D., "Finite Element Analysis of Wave Diffraction by a Crack," *Journal of the Engineering Mechanics Division*, ASCE, Vol. 102, No. EM3, Proc. Paper 12220, June, 1976, pp. 479–496.
3. Brown, K. M., and Dennis, J. E., "Derivative Free Analogues of the Levenberg-Marquardt and Gauss Algorithms for Nonlinear Least-Squares Approximation," *Numerische Mathematik*, Vol. 18, 1972, pp. 289–297.
4. Cedolin, L., and Dei Poli, S., "Finite Element Studies of Shear-Critical R/C Beams," *Journal of the Engineering Mechanics Division*, ASCE, Vol. 103, No. EM3, Proc. Paper 12968, June, 1979, pp. 395–410.
5. Cervenka, V., and Gerstle, K. H., "Inelastic Analysis of Reinforced Concrete Panels," *Publications*, International Association for Bridge and Structural Engineering, Zurich, Switzerland, Vol. 31, 1971, pp. 31–45, and Vol. 32, 1972, pp. 25–39.
6. Chen, S. K., Tuba, I. S., and Wilson, W. K., "On the Finite Element Method in Linear Fracture Mechanics," *Engineering Fracture Mechanics*, Vol. 6, 1970, pp. 159–167.
7. Gross, B., Roberts, E., and Srawley, J., "Elastic Displacements for Various Edge-Cracked Plate Specimens," *International Journal of Fracture Mechanics*, Groningen, Netherlands, Vol. 4, No. 3, Sept., 1968, pp. 267–275; Errata, Vol. 6, 1970, p. 87.
8. Hawkins, N. M., Wyss, A. N., and Mattock, A. H., "Fracture Analysis of Cracking in Concrete Beams," *Journal of the Structural Division*, ASCE, Vol. 103, No. ST5, Proc. Paper 12921, May, 1977, pp. 1015–1030.
9. Hellen, K. T., "On the Method of Virtual Crack Extensions," *International Journal for Numerical Methods in Engineering*, Vol. 9, 1975, pp. 187–207.
10. Hilton, P. D., and Sih, G. C., "Applications of the Finite Element Method to the Calculation of Stress Intensity Factors," *Methods of Analysis and Solutions of Crack Problems*, G. C. Sih, ed., Noordhoof Instructional Publishers, Leyden, Netherlands, 1973.
11. Kaplan, M. F., "Crack Propagation and the Fracture of Concrete," *American Concrete Institute Journal*, Vol. 58, No. 11, Nov., 1961.
12. King, W. W., et al., "Application of Running Crack Eigenfunctions to Finite-Element Simulation of Crack Propagation," *Mechanics Research Communications*, Vol. 3, 1976, pp. 197–202.
13. Knott, J. F., *Fundamentals of Fracture Mechanics*, Butterworths, London, England, 1973, p. 75.
14. Isida, M., "Stress-Intensity Factors for the Tension of an Eccentrically Cracked Strip," *Journal of Applied Mechanics*, American Society of Mechanical Engineers, Vol. 33, Series E, 1965, p. 674.
15. Marquardt, D. W., "An Algorithm for Least-Squares Estimation of Nonlinear Parameters," *Journal of the Society of Industrial and Applied Mathematics*, Vol. 2, No. 2, June, 1963, pp. 431–441.
16. Miyata, M., and Kusumoto, S., *Joint JSME-ASME Applied Mechanics Western Conference*, Japan Society of Mechanical Engineers, Tokyo, Japan, *Publication* No. A-12, 1975, pp. 383–390.
17. Ngo, D., and Scordelis, A. C., "Finite Element Analysis of Reinforced Concrete Beams," *Journal of the American Concrete Institute*, Vol. 66, No. 3, Mar., 1967, pp. 152–153.
18. Oglesby, J. J., and Lomacky, O., "An Evaluation of Finite Element Methods for the Computation of Stress Intensity Factors," *Journal of Engineering for Industry*, American Society of Mechanical Engineers, Vol. 95, 1973, pp. 177–185.
19. Parks, D. M., "A Stiffness Derivative Finite Element Technique for Determination of Crack Tip Stress Intensity Factors," *International Journal of Fracture Mechanics*,

Groningen, Netherlands, Vol. 10, 1974, pp. 487–502.
20. Rice, J. R., "An Examination of the Fracture Mechanics Energy Balance from the Point of View of Continuum Mechanics," *Proceedings*, First International Conference on Fracture, T. Yokobori, et al., eds., Japanese Society for Strength and Fracture of Materials, Tokyo, Japan, Vol. 1, 1965, pp. 309–340.
21. Rice, J. R., "Mathematical Analysis in the Mechanics of Fracture," *Fracture, an Advanced Treatise*, H. Liebowitz, ed., Vol. 2, Academic Press, New York, N.Y., 1968, pp. 191–250.
22. Scordelis, A. C., "Finite Element Analysis of Reinforced Concrete Structures," *Proceedings*, Specialty Conference on Finite Element Methods in Civil Engineering, McGill University, Montreal, Quebec, Canada, 1972, pp. 71–113.
23. Shah, S. P., and McGarry, F. J., "Griffith Fracture Criterion and Concrete," *Journal of the Engineering Mechanics Division*, ASCE, Vol. 97, No. EM6, Proc. Paper 8597, Dec., 1971, pp. 1163–1976.
24. Suidan, M., and Schnobrich, W. C., "Finite Element Analysis of Reinforced Concrete," *Journal of the Structural Division*, ASCE, Vol. 99, No. ST10, Proc. Paper 10081, Oct., 1973, pp. 2109–2122.
25. Tada, H., Paris, P. C., and Irwin, G. R., *The Stress Analysis of Cracks Handbook*, Del Research Corp., Hellertown, Pa., 1973.
26. Walsh, P. F., "Fracture of Plain Concrete," *The Indian Concrete Journal*, Vol. 46, Nov., 1972, pp. 469, 470, and 476.
27. Westergaard, H. M., *Journal of Applied Mechanics*, American Society of Mechanical Engineers, June, 1939, p. 49.
28. Williams, M. L., "On the Stress Distribution at the Base of a Stationary Crack," *Journal of Applied Mechanics*, Vol. 24, No. 1, Mar., 1957, pp. 109–114.
29. Wilson, W. H., "Finite Element Methods for Elastic Bodies Containing Cracks," *Methods of Analysis and Solutions of Crack Problems*, G. C. Sih, ed., Noordhoff International Publishers, Leyden, Netherlands, 1963, pp. 484–515.